Diffusion-Assisted Photoexcitation Transfer in Coupled Semiconducting Carbon Nanotube Thin Films

Maksim Grechko,[†] Yumin Ye,[‡] Randy D. Mehlenbacher,[†] Thomas J. McDonough,[†] Meng-Yin Wu,[§] Robert M. Jacobberger,[‡] Michael S. Arnold,[‡] and Martin T. Zanni[†,*]

[†]Department of Chemistry, University of Wisconsin—Madison, 1101 University Avenue, Madison, Wisconsin 53706, United States, [‡]Department of Materials Science and Engineering, University of Wisconsin—Madison, 1509 University Avenue, Madison, Wisconsin 53706, United States, and [§]Department of Electrical and Computer Engineering, University of Wisconsin—Madison, 1415 Engineering Drive, Madison, Wisconsin 53706, United States

ABSTRACT We utilize femtosecond transient absorption spectroscopy to study dynamics of photoexcitation migration in films of semiconducting single-wall carbon nanotubes. Films of nanotubes in close contact enable energy migration such as needed in photovoltaic and electroluminescent devices. Two types of films composed of nanotube fibers are utilized in this study: densely packed and very porous. By comparing exciton kinetics in these films, we characterize excitation transfer between carbon nanotubes inside fibers *versus* between fibers. We find that intrafiber transfer takes place in both types of films, whereas interfiber transfer is greatly suppressed in the porous one. Using films with different nanotube composition, we are able to test several models of exciton transfer. The data are inconsistent with models that rely on through-space interfiber energy transfer. A model that fits the experimental results postulates that interfiber transfer occurs only at intersections between fibers, and the excitons reach the intersections by diffusing along the long-axis of the tubes. We find that time constants for the inter- and intrafiber transfers are 0.2−0.4 and 7 ps, respectively. In total, hopping between fibers accounts for about 60% of all exciton downhill transfer prior to 4 ps in the dense film. The results are discussed with regards to transmission electron micrographs of the films. This study provides a rigorous analysis of the photophysics in this new class of promising materials for photovoltaics and other technologies.

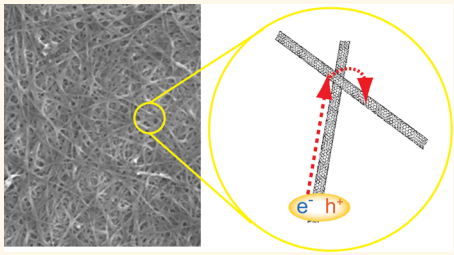

KEYWORDS: carbon nanotube · exciton · transient absorption · diffusion · electronic energy transfer · photovoltaic

The ability to separate carbon nanotubes by band gap and electronic type has enabled new investigations into the physics of energy transfer between semiconducting tubes. By centrifugation, selective chemistry, and other techniques,[1−5] it is now possible to make mixtures of chirality-specific nanotubes that are spectroscopically well isolated. Mixtures of nanotubes with controlled band gaps that are free of metallic tubes enable the physics of energy transfer to be studied between semiconducting tubes, providing insight into fundamental physics of electronic energy transfer between 1D systems as well as characterization of efficiencies for upcoming technologies, such as the use of nanotubes in photovoltaics[6−13] or electroluminescent devices.[14] Photoexcitation transfer between semiconducting single-wall carbon nanotubes (s-SWCNTs) in many environments has been addressed by different groups both experimentally and theoretically.[15−17] Efficient steady-state energy transfer to small band gap tubes was observed in pairs of nanotubes[18,19] as well as larger bundles[20−23] by monitoring photoluminescence. Time-resolved luminescence[24,25] and transient absorption[26,27] measurements on nanotube bundles revealed very short, from ∼500 fs down to 10 fs, transfer time. Nevertheless, little is known about exciton transfer between bundles in nanotube films and networks. Diffusion lengths of 3−7 nm across the film of polymer-wrapped s-SWCNTs has been estimated indirectly.[8,28] The rate and mechanism of exciton transfer between the bundles is still unclear due to the lack of direct time-resolved measurements. Exciton transfer between bundles of nanotubes will be a characteristic of next generation solar cells that use carbon nanotubes not only to transport charge but to absorb light, as well, which is the motivation of this work.

* Address correspondence to zanni@chem.wisc.edu.

Received for review August 9, 2013 and accepted May 7, 2014.

Published online May 07, 2014
10.1021/nn4041798

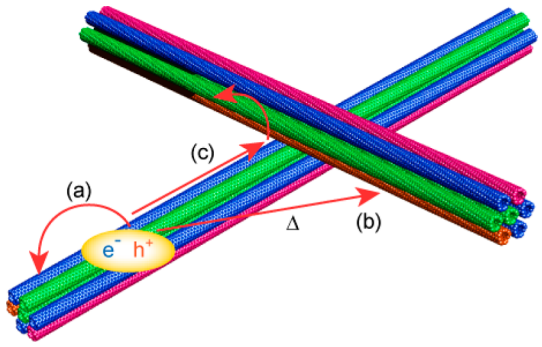

Figure 1. Layout of a nanotube film. Fibers consist of polymer-wrapped (not shown) nanotubes. The distance between fibers, Δ, is approximated by the fiber diameter ~5−10 nm in doctor-bladed films[17] and is much greater in critical point dried, more porous films. Exciton transfer: (a) intrafiber, (b) through-space interfiber, (c) diffusion-assisted interfiber.

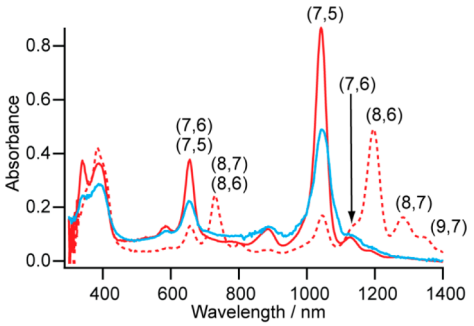

Figure 2. Absorbance spectra of carbon nanotube thin films. Films are prepared by CPD depositing a mixture of (7,5), (7,6), (8,6), (8,7), and (9,7) nanotubes (sample A, dashed red); CPD depositing a mixture enriched in (7,5) nanotubes (sample C, solid red); and doctor-blading a mixture enriched in (7,5) nanotubes (sample D, solid blue).

s-SWCNTs are an attractive light-harvesting material for applications in photovoltaic devices. Large absorption cross sections, transitions tunable across the solar spectrum, excellent charge transport, and high chemical stability make them a promising material for next generation solar cells.[6−13] Internal quantum efficiencies (IQE) >80% have been demonstrated for photovoltaic devices using bilayered s-SWCNT/C_{60} heterojunctions with a film thickness of ~4 nm.[28] However, IQEs are much lower in thicker films which are needed for more efficient light uptake.[28] In this work, we study the physics of exciton hopping in s-SWCNT thin films to better understand the factors that affect the IQE.

To be used as the light-absorbing material in bilayered solar cells, the semiconducting tubes must be deposited into a film. During a deposition process, tubes self-assemble into fibers (or bundles) (Figure 1). The spacing and diameter of the bundles in the film varies depending on the deposition method. For charge separation to occur, photoexcitation must transfer across bundles to reach the heterojunction. The purpose of this paper is to better understand the efficiency, time, and length scales associated with transfer through the film. In our recent work, we measured photoexcitation dynamics in films prepared by doctor-blade casting.[29] The morphology of these films is similar to those used in bilayered photovoltaic devices, consisting of an interwoven mat of fibers of hexagonally packed individually polymer-wrapped nanotubes.[28] The fibers were 5−10 nm in diameter, and the film was composed of a mixture of the (7,5), (7,6), (8,6), (8,7), and (9,7) nanotubes with band gaps in the range of 0.93−1.17 eV. We observed rapid exciton transfer from large to small band gap tubes, and we suggested several possible mechanisms by which this hopping could occur. However, there are multiple competing processes, namely, intra- and interband relaxation as well as intertube exciton transfer, which made it difficult to rigorously measure the time scales for each. In this paper, we report measurements on three new films. One film is made from the same mixture of carbon nanotubes as before but is prepared using critical point drying (CPD). CPD yields extremely porous films with substantially larger interfiber separation.[30] Thus, by comparison of CPD to doctor-bladed films, we explore the dependence of exciton migration on the film morphology. The other two films are made almost exclusively from (7,5) nanotubes, one of which is prepared by CPD and the other is doctor-bladed. The (nearly) single chirality films minimize energy transfer to tubes of different chiralities and thus simplify the kinetic scheme. Through a comparison of these three new samples and the original, we are able to quantitatively model the intertube exciton transfer, leading us to conclude that photoexcitation transfer in s-SWCNTs thin films can be well described by an intratube diffusion-assisted mechanism.

RESULTS AND DISCUSSION

Four types of samples discussed in this work are referenced as follows: sample A (7,5), (7,6), (8,6), (8,7), and (9,7) tubes CPD film; sample B (7,5), (7,6), (8,6), (8,7), and (9,7) tubes doctor-bladed film; sample C (7,5)-enriched CPD film; sample D (7,5)-enriched doctor-bladed film. Absorption spectra of samples A, C, and D are shown in Figure 2, whereas sample B has been measured previously (reproduced in Figure S1, Supporting Information).[29] The peak positions of E_{11} and E_{22} optical transitions in doctor-bladed and CPD films match exactly, from which we conclude that doctor-blading and CPD both create films with similar nanotube electronic structure. The E_{22} transitions have very similar line widths in both films, while the E_{11} transitions are ~30% broader in doctor-bladed film. The line widths of the doctor-bladed films are consistent with previous reports.[28] Broader transitions are most likely an indicator of differences in the dielectric environment.

While the electronic structure is similar between the films, the film morphologies are very different, as characterized by scanning electron microscopy (SEM) (Figure 3). The fibers in the doctor-bladed films are

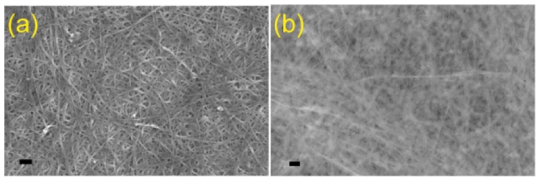

Figure 3. SEM images for (a) doctor-blading and (b) CPD-prepared films. Scale bars are 200 nm.

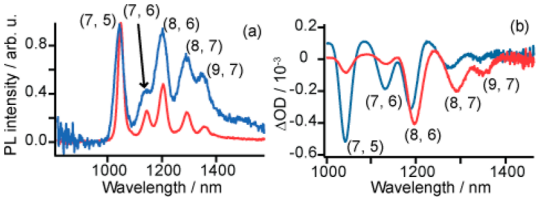

Figure 4. (a) Photoluminescence spectra of carbon nanotubes dispersed in solution (red) and CPD film (blue). (b) Transient absorption spectra of sample A at $t = -0.5$ ps (blue) and 10 ps (red) measured at magic angle.

packed about 100× more densely than in the CPD films. A doctor-bladed film of several nanometers has a similar optical density to a ~1 μm film prepared by CPD. Thus, the interfiber spacing in the CPD films is dramatically larger than that in the doctor-bladed films. In contrast, the fiber diameters are about the same at 5−10 nm, according to transmission electron microscopy (TEM) images (Figure S2, Supporting Information) and published results.[17] Thus, doctor-blading and CPD-prepared films result in approximately the same number of tubes per fiber.

On the basis of the considerable difference in film morphology, we might expect the films to exhibit different exciton kinetics. Shown in Figure 4a is a comparison of steady-state photoluminescence (PL) spectra of sample A and a dilute solution of nanotubes in chlorobenzene. In both samples, the E_{22} transitions of the (7,5) and (7,6) tubes are resonantly excited and the E_{11} photoluminescence is measured. In solution, little exciton transfer occurs because the tubes are spaced far apart (~1 μm). This is why the intensity of the PL is largest for the (7,5) tubes that are excited. In the film, the spectral weight of the PL shifts toward (8,6), (8,7), and (9,7) frequencies, which is evidence of exciton population transfer. A similar shift is observed for doctor-bladed films (Figure S3, Supporting Information).[29] Thus, photoexcitation transfer occurs between nanotubes of different diameters, regardless of whether the films were prepared by CPD or doctor-blading.

To resolve the dynamics of photoexcitation, we employ transient absorption spectroscopy. As for photoluminescence above, the E_{22} transitions of (7,5) and (7,6) tubes are resonantly excited by ~300 fs (fwhm) pump pulse and the E_{11} band gap transitions are probed using a white light pulse delayed by t. Control over pump polarization allows us to measure orientation dynamics associated with photoexcitation transfer

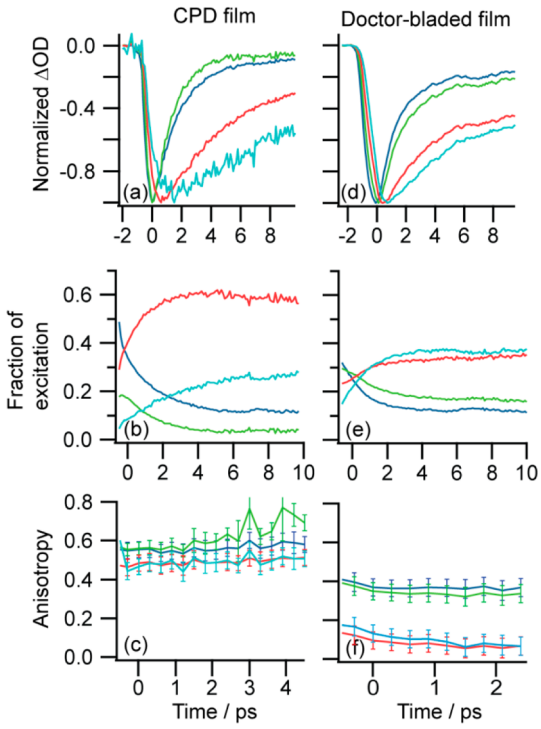

Figure 5. Kinetics traces measured for sample A: (a) normalized transient absorption intensities for each chirality nanotube; (b) fraction of total photoexcitation as a percentage of remaining photobleach on each chirality nanotube; (c) anisotropy kinetics for each chirality nanotube. Kinetics data for sample B in (d−f) are reproduced from ref 29 and correspond to (a−c), respectively. In all plots blue, green, red, and cyan are assigned for (7,5), (7,6), (8,6), and (8,7) tubes, respectively.

between tubes or to measure population kinetics that are independent of orientation (by setting the polarization at 45°, which is magic angle for a two-dimensional film[29]).

Shown in Figure 4b are transient absorption spectra of sample A collected at magic angle at $t = -0.5$ and 10 ps (we set $t = 0$ at the maximum of the photobleach of the (7,5) tubes and thus $t = -0.5$ ps occurs at the leading edge of the pump pulse). The spectral weight shifts from the resonantly excited (7,5) and (7,6) tubes to the (8,6), (8,7), and (9,7) tubes, indicating photoexcitation transfer. Kinetics for each size nanotube are shown in Figure 5a,b, which have a fast, subpicosecond transfer followed by a slower, few picosecond component. Thus, photoexcitation is transferring from larger to smaller band gap tubes on a femtosecond-to-picosecond time scale, similar to the doctor-bladed sample B (ref 29 and Figure 5d,e). Anisotropy measurements for sample A are shown in Figure 5c, calculated assuming that the nanotubes lie in a 2D plane. All tubes have an anisotropy near 0.5, which is time-independent. This indicates that excitons are transferred without change in their orientation. Since the CPD films are approximately as thick as the nanotubes are long and so may not be perfectly planar, we also calculated the anisotropy for a 3D distribution from which we reach the same conclusion (Figure S4a, Supporting Information).

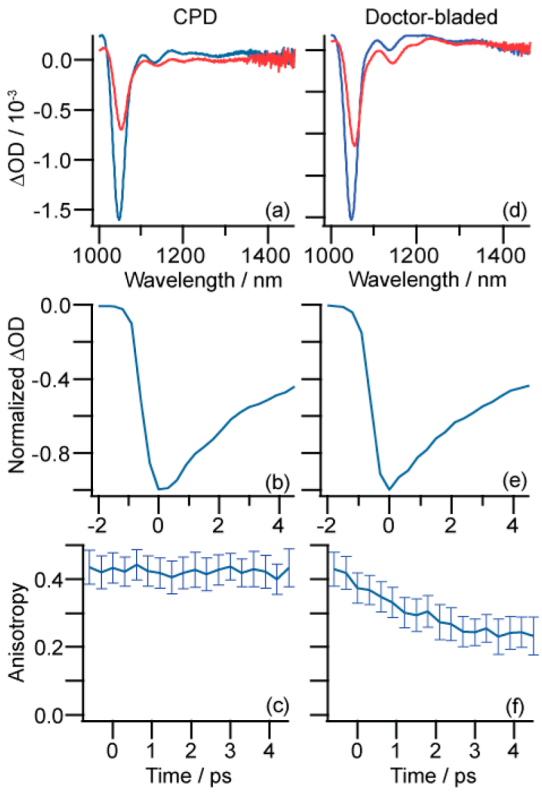

Figure 6. Transient absorption spectra of samples C (a) and D (d) at $t = 0$ (blue) and 5 ps (red). Kinetic traces of (7,5) tubes for samples C (b) and D (e). Anisotropy time traces of (7,5) tubes for samples C (c) and D (f).

The most likely way in which excitons can transfer between tubes without changing the anisotropy is if transfer is occurring inside fibers but not between fibers. Nanotubes in the same bundle will be parallel over very large distances, so if an exciton hops from one tube to another in the same bundle, its frequency will change but not the direction of its transition dipole. These observations in porous films are in stark contrast to our previously published work using doctor-blading in which hopping occurred between bundles (ref.29 and Figure 5f) in dense films. When a film is made from the same mixture of nanotubes but with doctor-blading, the population kinetics are very similar but the anisotropies decay on femtosecond-to-picosecond time scales. That data were explained by photoexcitation transfer between bundles since the bundles are randomly oriented in the plane, leading to a loss in anisotropy. Thus, exciton transfer occurs between carbon nanotubes in both CPD and doctor-bladed films, but in CPD films, transfer is confined to inside bundles because the large spacing between bundles suppresses interfiber transfer.

Shown in Figure 6a,d are transient absorption spectra at $t = 0$ and 5 ps for samples C and D, which are primarily composed of (7,5) tubes that are CPD and doctor-bladed, respectively. The E_{11} bleach of (7,5) tubes at ≈1050 nm dominates the spectra at all time delays for both samples. Weak signal at ≈1135 nm is most likely generated by the small fraction of (7,6) nanotubes contained in the samples. Kinetic plots of the (7,5) tubes decay exponentially (Figure 6b,e), but they are not a good measure of excitation transfer since all tubes absorb at the same frequency. Thus, in these single chirality films, anisotropy is the best indicator of exciton transfer. To within the error bars, we find that the anisotropy of sample C is constant, which is consistent with the results of sample A above that CPD preparation prevents hopping between bundles (Figure 6c and Supporting Information Figure S4b). In contrast, the anisotropy of sample D monotonically decays from 0.42 to 0.23 over 5 ps, indicating that exciton hopping is occurring between bundles in the doctor-bladed samples (Figure 6f). It also shows that hopping occurs between nanotubes of the same chirality. Thus, downhill energy transfer is not necessary for hopping. The moderate anisotropy decrease of the sample D strikingly differs from the abrupt, sub-100 fs, drop to 0.15 when excitons are transferred between tubes of different chiralities (ref 29 and Figure 5f). The simulations below quantify these observations.

In summary of our experimental data, we learn that (1) photoexcitation transfer occurs between carbon nanotubes inside bundles, which we refer to as intrafiber hopping; (2) transfer occurs between bundles, which we call interfiber hopping; and (3) transfer occurs between carbon nanotubes of the same band gap as well as to the tubes of smaller band gap. From our previous work, we knew that interfiber hopping occurred, but we could not deconvolve it from these other transfer processes.[29] With this additional data, we can now simulate and test a variety of models for exciton transfer to obtain more quantitative insight into the photoexcitation transfer pathways.

Simulations of Photoexcitation Transfer. We test four models for exciton transfer in s-SWCNTs thin films that might explain our data. Our hypothesis is that diffusion of excitons along the fibers is necessary to describe the kinetics. We test three models to evaluate if the kinetics of the doctor-bladed films can be described by through-space coupling (for example *via* Förster-like energy transfer), excluding intratube exciton diffusion. A fourth model is tested that includes intratube exciton diffusion to the points where fibers are touching, followed by interfiber transfer. To test the models, we simulate the anisotropy and population of the tubes as a function of time for measurements of samples B and D. Only the doctor-bladed samples B and D are needed to obtain a stringent test between simulation and experiment. Each model has its own approximations, but for all models, we assume that (7,5) and (7,6) tubes are identical since both are resonant with the pump pulse. Thus, we merge their kinetics and refer to them

as {7}. For each polarization condition, the transient absorption intensity of {7} is given by the sum of intensities of (7,5) and (7,6) tubes. Anisotropy of {7} is calculated using intensities obtained for parallel and perpendicular polarizations of the pump and probe. Similarly, (8,6) and (8,7) tubes are referenced as {8}. The (9,7) tubes are ignored because they contribute only 3% to the sample and their signal is barely noticeable in transient absorption spectra, which indicates that the fraction of excitons on them is very small.[29] In none of the models do we consider free charge carriers. Free carriers can be generated by E_{22} excitation,[31] but it has been shown that exciton-only models are sufficient to reproduce dynamics of s-SWCNTs up to tens of picoseconds.[32] We simulate data up to 5 ps because by that time 70% of the excitons have transferred to the two lowest band gap tubes. These excitons are of particular interest because they are probably responsible for the very high IQE of photovoltaic devices fabricated from s-SWCNTs (>80%). As we demonstrate below, only the fourth model that involves intratube exciton diffusion prior to transferring between bundles agrees well with our experiments. From the fits, we obtain intra- and interfiber transfer rates that provide a comprehensive kinetic mechanism for transfer in the carbon nanotube thin film. After analyzing the doctor-bladed samples, we discuss the results of the CPD samples A and C.

Model 1: Through-Space Resonance Energy Transfer. In this first model, we test whether through-space resonance energy transfer (RET) can account for the observed dynamics of the doctor-bladed films. For exciton transfer between fibers, we utilize a conventional RET rate constant given by[16,33]

$$k(\alpha) = \frac{2\pi}{\hbar}|V(\alpha)|^2 J \qquad (1)$$

where $V(\alpha)$ is coupling between tubes at angle α and J is spectral overlap between their transitions. At an interfiber separation of 5−10 nm (Figure 1), interfiber orbital overlap should be negligible. Therefore, Columbic interactions can be used to describe the coupling. We use $V(\alpha) \propto \cos(\alpha)$ consistent with a dipole coupling model due to the significant, 5−10 nm, distance between fibers in the doctor-bladed films. No significant {8}-to-{7} transfer was observed in experiment,[29] thus it is set to zero. The rate constants for {7}-to-{7} and {8}-to-{8} transfer are assumed to be equal due to the equal (within 5%) oscillator strengths.[34]

The intrafiber transfer occurs between parallel tubes and is introduced by its rate constant. The exact mechanism of the intrafiber transfer is not important for the following discussion. For our model, the master equations for exciton transfer in the plane of the film have the following form (see Supporting Information for details):

$$\begin{aligned}
\frac{\partial n_{\{7\}}(\theta,t)}{\partial t} &= \frac{1}{\pi}G_{\{7\}}\int_0^{\pi} k^{\text{inter}}_{\{7\}\rightarrow\{7\}}(\theta-\varphi)n_{\{7\}}(\varphi,t)\mathrm{d}\varphi \\
&\quad -\frac{1}{\pi}G_{\{7\}}n_{\{7\}}(\theta,t)\int_0^{\pi} k^{\text{inter}}_{\{7\}\rightarrow\{7\}}(\theta-\varphi)\mathrm{d}\varphi \\
&\quad -\frac{1}{\pi}G_{\{8\}}n_{\{7\}}(\theta,t)\int_0^{\pi} k^{\text{inter}}_{\{7\}\rightarrow\{8\}}(\theta-\varphi)\mathrm{d}\varphi \\
&\quad -k^{\text{intra}}_{\{7\}\rightarrow\{8\}}G_{\{8\}}n_{\{7\}}(\theta,t) \\
\frac{\partial n_{\{8\}}(\theta,t)}{\partial t} &= \frac{1}{\pi}G_{\{8\}}\int_0^{\pi} k^{\text{inter}}_{\{8\}\rightarrow\{8\}}(\theta-\varphi)n_{\{8\}}(\varphi,t)\mathrm{d}\varphi \\
&\quad -\frac{1}{\pi}G_{\{8\}}n_{\{8\}}(\theta,t)\int_0^{\pi} k^{\text{inter}}_{\{8\}\rightarrow\{8\}}(\theta-\varphi)\mathrm{d}\varphi \\
&\quad +\frac{1}{\pi}G_{\{8\}}\int_0^{\pi} k^{\text{inter}}_{\{7\}\rightarrow\{8\}}(\theta-\varphi)n_{\{7\}}(\varphi,t)\mathrm{d}\varphi \\
&\quad +k^{\text{intra}}_{\{7\}\rightarrow\{8\}}G_{\{8\}}n_{\{7\}}(\theta,t)
\end{aligned} \qquad (2)$$

Here $n_{\{7\}}(\theta,t)$ ($n_{\{8\}}(\theta,t)$) is time-dependent angular distribution of excitons residing on {7} ({8}), θ is the angle between the transition dipole moment of the exciton and the polarization of the pump pulse, $G_{\{7\}}$ ($G_{\{8\}}$) is the number of quantum states of {7} ({8}) available for the exciton to hop to; $k^{\text{inter}}_{\{7\}\rightarrow\{7\}}$, $k^{\text{inter}}_{\{8\}\rightarrow\{8\}}$, $k^{\text{inter}}_{\{7\}\rightarrow\{8\}}$, and $k^{\text{intra}}_{\{7\}\rightarrow\{8\}}$ are rate constants for interfiber {7}-to-{7}, {8}-to-{8}, {7}-to-{8}, and intrafiber {7}-to-{8} transfer, respectively. Generally speaking, eqs 2 should include exciton recombination terms. So that we do not need to explicitly include lifetimes, in the following, we model the fraction of remaining photobleach on each chirality nanotube instead of the absolute photobleach intensity. This fraction is calculated as a ratio of the signal generated by specific type of tubes to a sum of signals from all the tubes at a given time delay. Because of chirality-independent recombination rates,[29] the kinetics of these fractions solely represent population transfer between different tubes; therefore the recombination term is omitted in eqs 2. When {7} is selectively excited by linearly polarized light the boundary conditions are given by

$$\begin{aligned} n_{\{7\}}(\theta,0) &= \cos^2(\theta) \\ n_{\{8\}}(\theta,0) &= 0 \end{aligned} \qquad (3)$$

The anisotropy $A(t)$ is calculated using eq 4 for a 2D sample because doctor-bladed films are only several nanometers thick:

$$A_r(t) = \frac{\int_0^{\pi} n_r(\theta,t)(\cos^2(\theta,t) - \sin^2(\theta,t))\mathrm{d}\theta}{\int_0^{\pi} n_r(\theta,t)(\cos^2(\theta,t) + \sin^2(\theta,t))\mathrm{d}\theta} \qquad (4)$$

where r = {7} or {8}. To obtain the rate constants, we first use eqs 2−4 to fit the anisotropy kinetics of sample D as best as possible because the fit requires only the first equation of eqs 2 with $G_{\{8\}} = 0$ and so there is only one unknown, $k^{\text{inter}}_{\{7\}\rightarrow\{7\}}(\theta)\, G_{\{7\}}$. The fit reproduces well the slope of the anisotropy decay but is offset by ~0.07 at all time delays (Figure 7a). This offset stems from the boundary conditions, which predicts an initial

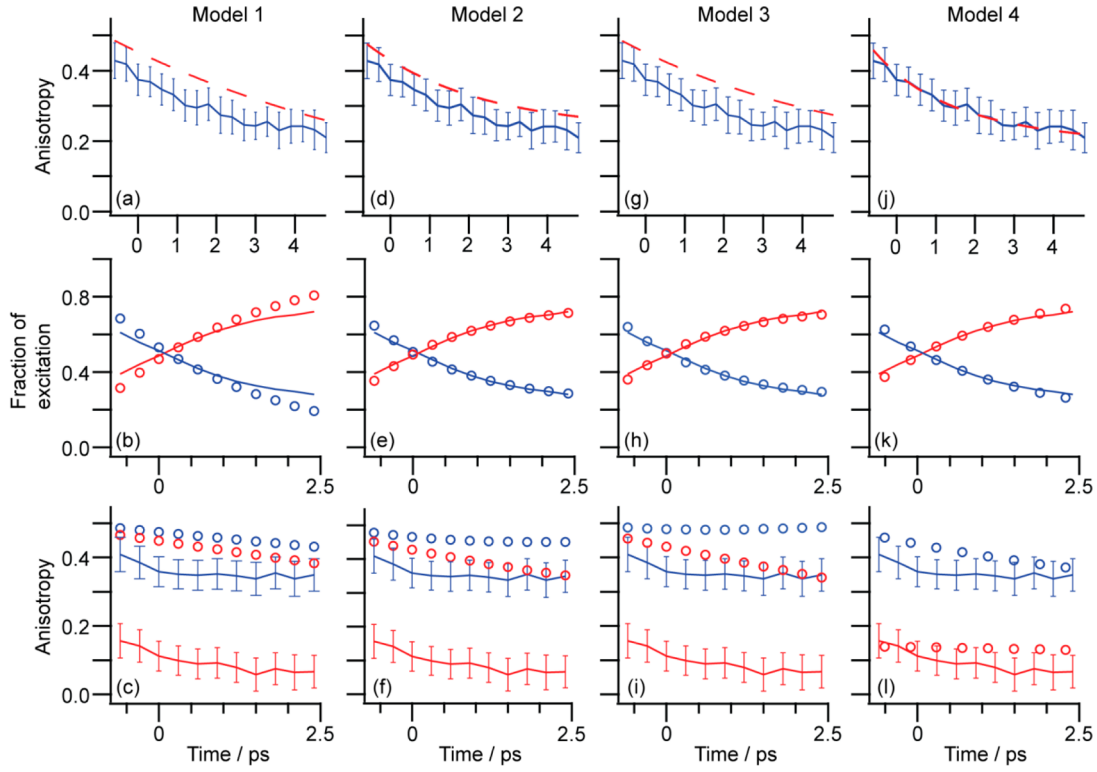

Figure 7. (a,d,g,j) Fit of anisotropy kinetics of {7} (dashed red) to anisotropy kinetics of sample D (solid blue) using models 1−4. (b,e,h,k) Fit of population evolution calculated using models 1−4 (circles) for {7} (blue) and {8} (red) to population kinetics of sample B (solid lines). (c,f,i,l) Comparison of the simulated anisotropy kinetics (circles) for {7} (blue) and {8} (red) using models 1−4 with experimental data (solid lines).

anisotropy of 0.5, whereas the experimental value is ~0.43. Thus, while the fit is not perfect, we obtain the interfiber transfer rate $k^{\text{inter}}_{\{7\}\rightarrow\{7\}}(0)G^{\text{D}}_{\{7\}} = 0.47\ \text{ps}^{-1}$, where superscript D denotes the sample.

Having estimated interfiber transfer rates, we turn to sample B to obtain intrafiber rates between different diameter nanotubes, $k^{\text{intra}}_{\{7\}\rightarrow\{8\}}(0)G_{\{8\}}$. First, we note that sample B is composed of {7} and {8} in a ratio of 1/2,[29] thus

$$k^{\text{inter}}_{\{7\}\rightarrow\{7\}}(0)G^{\text{B}}_{\{7\}} = \frac{1}{3}k^{\text{inter}}_{\{7\}\rightarrow\{7\}}(0)G^{\text{D}}_{\{7\}} = 0.16\text{ps}^{-1}$$
$$k^{\text{inter}}_{\{8\}\rightarrow\{8\}}(0)G^{\text{B}}_{\{8\}} = \frac{2}{3}k^{\text{inter}}_{\{7\}\rightarrow\{7\}}(0)G^{\text{D}}_{\{7\}} = 0.31\text{ps}^{-1} \quad (5)$$

in which we have used our assumption that the rate constants for {7}-to-{7} and {8}-to-{8} transfer are equal. To derive intrafiber rates for different chiralities, $k^{\text{intra}}_{\{7\}\rightarrow\{8\}}(0)G_{\{8\}}$, we fit the population fraction kinetics of sample B measured at magic angle. At magic angle, the intensity of each tube is proportional to the number of excitons on it and is independent of exciton orientational dynamics. Fractions of excitons residing on {7} and {8} are given by

$$f_r(t) = \frac{\int_0^{\pi} n_r(\theta,t)\text{d}\theta}{\int_0^{\pi} n_{\{7\}}(\theta,t)\text{d}\theta + \int_0^{\pi} n_{\{8\}}(\theta,t)\text{d}\theta} \quad (r = \{7\},\{8\}) \quad (6)$$

$f_r(t)$ depends on both intra- and interfiber transfer. As it turns out, $k^{\text{inter}}_{\{7\}\rightarrow\{8\}}$ has little impact on the simulations. Because resonant energy transfer scales with the coupling which should decrease rapidly with the distance between tubes;[16,19] $k^{\text{inter}}_{\{7\}\rightarrow\{8\}}$ must be significantly smaller than $k^{\text{intra}}_{\{7\}\rightarrow\{8\}}$. For example, setting it to one-third or one-tenth the intrafiber rate (*e.g.*, $k^{\text{inter}}_{\{7\}\rightarrow\{8\}}(0) = (1/3)k^{\text{intra}}_{\{7\}\rightarrow\{8\}}$ and $k^{\text{inter}}_{\{7\}\rightarrow\{8\}}(0) = (1/10)k^{\text{intra}}_{\{7\}\rightarrow\{8\}}$), only changes from $k^{\text{intra}}_{\{7\}\rightarrow\{8\}}G^{\text{B}}_{\{8\}} = 0.36\ \text{ps}^{-1}$ to $k^{\text{intra}}_{\{7\}\rightarrow\{8\}}G^{\text{B}}_{\{8\}} = 0.4\ \text{ps}^{-1}$, respectively. This is also true in models 2 and 3 below, as well as for the anisotropy simulations (see Figure S5, Supporting Information), and so in models 1−3, we use $k^{\text{inter}}_{\{7\}\rightarrow\{8\}}(0) = (1/10)k^{\text{intra}}_{\{7\}\rightarrow\{8\}}$ (the fit is shown in Figure 7b).

Finally, having obtained values for both intra- and interfiber transfer rates, we model the anisotropy of sample B using eq 4, which is plotted in Figure 7c. The anisotropy of {7} is still too large, as expected from the fits to sample D. More importantly, the anisotropy predicted for {8} is ≳0.4, which is vastly larger than experiment. We note that utilization of $V(\alpha)$ dependence predicted by Wong *et al.*[16] for 0.3 nm wall-to-wall distance between the tubes results in larger discrepancy between theory and experiment (not shown) due to more rapid decrease of coupling strength with the angle between the tubes. Even if we relax the assumption of the $V(\alpha) \propto \cos(\alpha)$ angular dependence to allow equal transfer regardless of orientation, the anisotropy is still not reproduced (Figure S6, Supporting Information). Thus, this model

does not properly account for the loss of anisotropy that accompanies hopping between different chiralities.

Model 2: Through-Space Resonance Energy Transfer with Exciton Trapping. It has been hypothesized that excitons can become trapped at defect sites in carbon nanotubes,[35−38] which our previous model does not take into account. In experiment, there is decrease of apparent interfiber hopping rate with waiting time, as observed in the population fractions (Figure 5b,e). Most of the excitons are transferred within 2 ps, whereas after 4 ps exciton, distribution is almost constant. This might be attributed to the exciton trapping because trapped excitons will still generate photobleach even if they do not transfer. To take trapping into account, we modify model 1 with an additional rate constant, k_{tr}. We assume that trapping can occur on either $\{7\}$ or $\{8\}$ and that mobile and trapped excitons have equal probabilities for both nonradiative and radiative recombination. In this model, eqs 2 are modified to include a trapping term:

$$\frac{\partial n_r^m(\theta, t)}{\partial t} = \ldots - k_{tr} n_r^m(\theta, t)(r = \{7\}, \{8\}) \quad (7)$$

where superscript m denotes mobile excitons. Two more equations are needed to describe trapped photoexcitations denoted by superscript t:

$$\frac{\partial n_r^t(\theta, t)}{\partial t} = k_{tr} n_r^m(\theta, t)(r = \{7\}, \{8\}) \quad (8)$$

The anisotropy must be calculated using the photobleach of both the mobile and trapped excitons:

$$A_r(t) = \frac{\int_0^{\pi} (n_r^m(\theta, t) + n_r^t(\theta, t))(\cos^2(\theta) - \sin^2(\theta))\mathrm{d}\theta}{\int_0^{\pi} (n_r^m(\theta, t) + n_r^t(\theta, t))(\cos^2(\theta) + \sin^2(\theta))\mathrm{d}\theta} \quad (9)$$

where $r = \{7\}$ or $\{8\}$. As in model 1, we then fit the anisotropies and population fractions for sample D and B to obtain values for $k^{inter}_{\{7\}\rightarrow\{7\}}(0)G^D_{\{7\}}$, $k^{intra}_{\{7\}\rightarrow\{8\}}G^B_{\{8\}}$, and now k_{tr}. The best fits are shown in Figure 7d,e, which has $k^{inter}_{\{7\}\rightarrow\{7\}}(0)G^D_{\{7\}} = 0.75$ ps^{-1}, $k^{intra}_{\{7\}\rightarrow\{8\}}G^B_{\{8\}} = 0.5$ ps^{-1}, and $k_{tr} = 0.16$ ps^{-1}. Clearly, exciton trapping does not improve the agreement of simulated anisotropy kinetics of sample B with experiment in Figure 7f.

Models 1 and 2 discussed above are insufficient to describe the data of sample B because they all predict an anisotropy of ≈0.5 at $t = -0.6$ ps, whereas the experimental values are 0.4 or 0.2. To reach those values within the confines of the model parameters, exceedingly fast exciton hopping between fibers is required. However, fast migration does not fit with data from sample D (Figure 6f) in which the anisotropy decays on a several picosecond time scale. Thus, these models cannot simultaneously reproduce the data from both samples B and D.

Model 3: Through-Space Resonance Energy Transfer with Initially Trapped Excitons. One way in which the RET models above might be modified to better agree with the data is if many of the initially generated excitons are immediately trapped. Trapped excitons generated by direct photoexcitation or on ultrafast, ≲100 fs, time scale can result in picosecond range anisotropy decay of $\{7\}$ even when mobile exciton hopping rate is fast enough to produce ≈100 fs anisotropy drop of $\{8\}$. In this model, trapped excitons are generated within the experimental time resolution (≲300 fs) and assumed to trap onto $\{7\}$ tubes. Equations 2 describe the dynamics of mobile excitons while the trapped fraction γ is an adjustable constant. Anisotropy is then given by eq 9. We determine $\gamma = 0.25$ from the fraction of excitons on $\{7\}$ at $t = 8$ ps (Figure 5e). Parameters are found by fitting, which gives $k^{inter}_{\{7\}\rightarrow\{7\}}(0)G^D_{\{7\}} = 0.66$ ps^{-1} and $k^{intra}_{\{7\}\rightarrow\{8\}}G^B_{\{8\}} = 0.69$ ps^{-1} (Figure 7g,h). Parameters in this model are ∼1.5 times larger than those derived in model 1 because now only 75% of photoexcitations are involved in the transfer process. Figure 7i presents simulated anisotropy kinetics of sample B. Disagreement with experiment in this figure is similar to previous models.

In models 1−3 above, $k^{inter}_{\{7\}\rightarrow\{8\}}$ was not allowed to be faster than $k^{intra}_{\{7\}\rightarrow\{8\}}$ because the average distance between nanotubes in a fiber is much smaller than the average distance between fibers. This physical constraint makes sense in models 1−3 because only one averaged rate is used for each kind of transfer. If we had allowed $k^{inter}_{\{7\}\rightarrow\{8\}}$ to be greater than $k^{intra}_{\{7\}\rightarrow\{8\}}$, the data could indeed be fit. This phenomenon could occur at fiber−fiber intersections. We know that the distances between nanotubes on different fibers can be quite close near fiber−fiber intersections, and so we hypothesize that, at fiber crossing points, $k^{inter}_{\{7\}\rightarrow\{8\}}$ is comparable to or even exceeds $k^{intra}_{\{7\}\rightarrow\{8\}}$, depending on the structure of the fiber intersections. Thus, we need a model that describes the kinetics of exciton transfer at these intersections and the transport of excitons to these intersections.

Model 4: Intratube Diffusion-Assisted Exciton Transfer. None of the 3 models discussed above can reproduce the experimental data. In order to explain the data, the intra- and interfiber transfer rates need to be about equal. The above models assume that interfiber transfer is slower because the bundles are separated by large distances. Thus, these models predict that transfer predominantly occurs between tubes in the same fiber, which does not change the anisotropy. No matter what the angular dependence of the transfer, this assumption produces much smaller interfiber transfer. Of course, in an actual film, the fibers cross at intersections in which the distances between tubes is much smaller than on average, and hence an exciton at the crossing point between tubes could have a higher probability of transferring. In the doctor-bladed film, the nanotubes cross about every ∼30 nm. We hypothesize

that at these points interfiber transfer will compete with intrafiber. Since there are few intersections compared to the lengths of the fibers, we also hypothesize that a generated exciton will usually travel before transferring. We call this exciton motion "intratube diffusion". Of course, excitons can still hop between nanotubes in the same fiber while they diffuse to the intersections. Thus, model 4 is a diffusion-assisted transfer model. Diffusion lengths of up to few hundred nanometers in s-SWCNTs make such a mechanism feasible.[32,39−48] According to this hypothesis, the interfiber transfer rate constant will depend on time, t, because an exciton travels along the nanotube before interfiber hopping. The master equations now become

$$\begin{aligned}\frac{\partial n_{\{7\}}(\theta,t)}{\partial t} &= k^{\text{inter}}_{\{7\}\rightarrow\{7\}}(t)[T_{\{7\}}]n_{\{7\}}(t)\\ -k^{\text{inter}}_{\{7\}\rightarrow\{7\}}(t)[T_{\{7\}}]n_{\{7\}}(\theta,t) &- k^{\text{inter}}_{\{7\}\rightarrow\{8\}}(t)[T_{\{8\}}]n_{\{7\}}(\theta,t)\\ &- k^{\text{intra}}_{\{7\}\rightarrow\{8\}}G_{\{8\}}n_{\{7\}}(\theta,t),\\ \frac{\partial n_{\{8\}}(\theta,t)}{\partial t} &= k^{\text{inter}}_{\{8\}\rightarrow\{8\}}(t)[T_{\{8\}}]n_{\{8\}}(t)\\ &- k^{\text{inter}}_{\{8\}\rightarrow\{8\}}(t)[T_{\{8\}}]n_{\{8\}}(\theta,t)\\ +k^{\text{inter}}_{\{7\}\rightarrow\{8\}}(t)[T_{\{8\}}]n_{\{7\}}(t) &+ k^{\text{intra}}_{\{7\}\rightarrow\{8\}}G_{\{8\}}n_{\{7\}}(\theta,t)\end{aligned} \tag{10}$$

$[T_{\{7\}}]/[T_{\{8\}}]$ is the concentration of crossing points with $\{7\}/\{8\}$, $n_{\{7\}/\{8\}}(t)$ is total number of excitons integrated over all angles on $\{7\}/\{8\}$.

At short time delays, $n_{\{8\}} \ll n_{\{7\}}$. Thus, in the second equation of eqs 10 we can ignore for the sake of discussion the first two terms on the right side:

$$\frac{\partial n_{\{8\}}(\theta,t)}{\partial t} \propto k^{\text{inter}}_{\{7\}\rightarrow\{8\}}(t)[T_{\{8\}}]n_{\{7\}}(t) + k^{\text{intra}}_{\{7\}\rightarrow\{8\}}G_{\{8\}}n_{\{7\}}(\theta,t) \tag{11}$$

According to eq 11, at short time delays, angular exciton distribution, $n_{\{8\}}(\theta,t)$, is determined by initial distribution of excitons on $\{7\}$, $n_{\{7\}}(\theta,t)$, and the ratio of inter- to intrafiber transfer rates, $k^{\text{inter}}_{\{7\}\rightarrow\{8\}}(t)\ [T_{\{8\}}]/k^{\text{intra}}_{\{7\}\rightarrow\{8\}}G_{\{8\}}$. If $k^{\text{inter}}_{\{7\}\rightarrow\{8\}}(t)\ [T_{\{8\}}] \gg k^{\text{intra}}_{\{7\}\rightarrow\{8\}}G_{\{8\}}$, excitons transferred to parallel tubes inside a fiber dominate and $n_{\{8\}}(\theta,t)$ is a replica of $n_{\{7\}}(\theta,t)$. In this case, the anisotropies of $\{8\}$ and $\{7\}$ match. Thus, the difference of anisotropies of $\{7\}$ and $\{8\}$ at short time delays has a simple physical meaning: it is a measure of the ratio of excitons transferred between fibers to those transferred inside a fiber.

To find how interfiber transfer rate constants depend on time we need to solve a 1D diffusion equation with certain boundary conditions. We postulate that the flux Φ of excitons transferred between fibers is proportional to the number of excitons within small distance d near the fiber touching point:[49]

$$\Phi(t) = \frac{c(x_0,t)d}{\tau^{\text{inter}}} \tag{12}$$

where $c(x,t)$ is concentration of excitons as a function of coordinate along a tube and time, x_0 is coordinate of a crossing point, and τ^{inter} is time constant of interfiber exciton hopping at the fiber crossing. We note that $n(t) = \int_S c(x,t)dx$, where S is the length of all tubes (angle is omitted for simplicity). By analogy with diffusion-limited contact quenching, we postulate that[40,50]

$$k^{\text{inter}}(t) = \left|\frac{D}{c_0}\frac{\partial c(x_0,t)}{\partial x}\right| \tag{13}$$

where c_0 is initial exciton concentration, $c(x,0) = c_0$. Solution of the diffusion equation with boundary condition given by eq 12 depends on d/τ^{inter}, distance L between the fiber intersections and diffusion coefficient D (see Supporting Information for details). For sample D, we use L = 30 nm estimated from SEM images of doctor-bladed films. We assume that there is one touching tube per crossing point per fiber. Thus, because of the dilution factor for sample B, we use L = 90 and 22.5 nm for the $\{7\}$-$\{7\}$ and $\{7\}/\{8\}$-$\{8\}$ crossings, respectively. Thus, for sample D $[T_{\{7\}}]$ = 2/30 nm^{-1} and for sample B $[T_{\{7\}}]$ = 2/90 nm^{-1}, $[T_{\{7\}}]$ = 2/22.5 nm^{-1} (factor 2 corresponds to 2 crossings at the ends of a free interval of a fiber). The reported diffusion coefficients of s-SWCNTs range from 0.1 to 10.7 cm^2 s^{-1}.[32,39,40,42,51] We use the average, D = 5 cm^2 s^{-1}. We fit the experimental data by varying $d/\tau^{\text{inter}}_{\{7\}\rightarrow\{7\}}$, $d/\tau^{\text{inter}}_{\{7\}\rightarrow\{8\}}$, and $k^{\text{intra}}_{\{7\}\rightarrow\{8\}}$.

From the fit (Figure 7j−l), we find $d/\tau^{\text{inter}}_{\{7\}\rightarrow\{8\}}$ = 10 ± 2 nm/ps and $k^{\text{intra}}_{\{7\}\rightarrow\{8\}}G_{\{8\}}$ = 0.15 ± 0.03 ps^{-1}. To find the time constant of interfiber hopping $\tau^{\text{inter}}_{\{7\}\rightarrow\{8\}}$, we approximate d by the size of the exciton, 2 nm,[51] because the diameters of the tubes used in this study are <2 nm. Thus, $\tau^{\text{inter}}_{\{7\}\rightarrow\{8\}} \approx 0.20 \pm 0.02$ ps. The intrafiber hopping time is $\tau^{\text{intra}} = 1/k^{\text{intra}}_{\{7\}\rightarrow\{8\}}G_{\{8\}} = 7 \pm 1$ ps. About 60% of excitons transferred downhill in the doctor-bladed films prior to 4 ps are transferred between fibers. Inter- and intrafiber transfer times are consistent with previously reported values of exciton transfer rates between bundled bare and polymer-wrapped s-SWCNTs, respectively.[25] Thus, we hypothesize that, at crossing points, nanotubes touch or are in closer proximity, on average, than for nanotubes in the same fiber.

Another interesting observation is that the interfiber $\{7\}$-to-$\{8\}$ and $\{7\}$-to-$\{7\}$ transfer time constants are not the same (0.2 ± 0.02s and 0.4 ± 0.02 ps, respectively). This difference may indicate that the coupling between tubes may depend on tube diameter. Alternatively, back transfer might take place between touching tubes of the same diameter because there is no exciton energy relaxation on the acceptor tube in this case. A back transfer process would decrease the apparent interfiber exciton flux and thus increase the apparent transfer time constant.

Applying Model 4 to CPD-Deposited Films. Having fit the data of the doctor-bladed film to test model 4 and extract rate constants, we now apply it to predict the

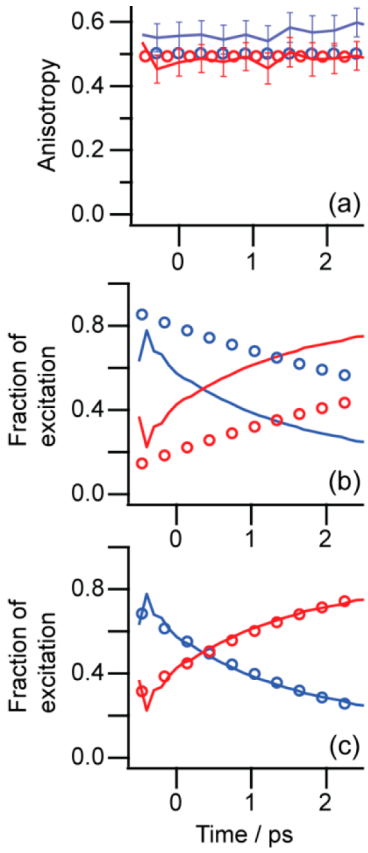

Figure 8. Comparison of the measured exciton kinetics for the CPD film with that predicted by model 4. In the simulations, the distance between fiber intersections is $L = 3$ μm. (a) Anisotropy and (b) fraction of excitation plotted against waiting time. Transfer rates utilized in these simulations are obtained from the fit of doctor-bladed films. (c) Fitting of the experiment using model 4. Traces for $\{7\}$ and $\{8\}$ are shown by blue and red, respectively. Simulations and experimental data are shown by circles and solid lines, respectively.

results expected for the CPD films. As discussed in the experimental section above, the interfiber spacing is about 100× larger than in the doctor-bladed films, resulting in a much lower density of intersection points. According to model 4, this difference would result in a suppression of the interfiber exciton transfer in CPD films due to the large distances between the tube intersections. Shown in Figure 8 are the resulting simulations. A 100-fold increase in the distance between the intersections completely eliminates interfiber transfer, as can be seen in the anisotropy measurements (Figure 8a). However, if the intrafiber transfer rates from the doctor-bladed film are used, the fraction of excitons does not match (Figure 8b); the intrafiber transfer rate derived for the doctor-bladed films is too small to reproduce the kinetics of the CPD films. To match the data, an intrafiber transfer rate of 0.36 ± 0.03 ps^{-1} is needed (Figure 8c), which is about 2.5 times faster than in the doctor-bladed films.

TEM Analysis of Fiber Structures: Comparison to Kinetics. The above analysis of the kinetics predicts that the

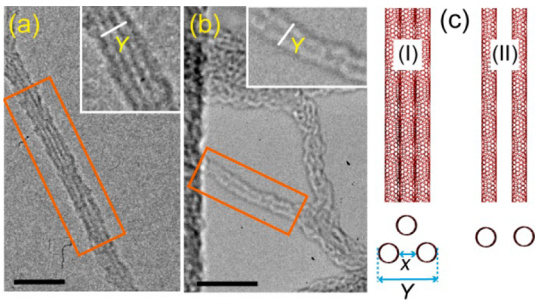

Figure 9. TEM images of fibers composed of (a) two or three nanotubes in doctor-blading and (b) two nanotubes in CPD-prepared films (orange boxes). (c) Layouts of fibers in (a) if fibers are composed of (I) three and (II) two nanotubes. Scale bars are 10 nm.

interfiber transfer rates are faster for doctor-bladed than for CPD films but slower for intrafiber transfer. The interfiber rate agrees with the porosity of the CPD films: the SEM of the films (Figure 3) shows a less dense network of fibers for CPD, implying fewer intersections. One interpretation for why the intrafiber transfer rates for the CPD films are faster is because the tubes are closer together in fibers preparered by CPD. To investigate this possibility, we collected TEM images of (7,5)-enriched films prepared by doctor-blading and CPD (Figure 9 and Supporting Information S7) and looked for fibers composed of only two or three nanotubes. Picking points along the fibers with high contrast, we measure distances across the bundle, Y, as shown in the insets. Because it is difficult to know if the fiber has 2 or 3 tubes in Figure 9a, we calculate the wall-to-wall distance using the two possible layouts shown in Figure 9c. Given that the diameter of (7,5) tubes is $d = 0.83$ nm, the wall-to-wall distance in doctor-bladed sample is $x = Y - 2d = 1.0 \pm 0.2$ nm, which is similar to distance previously observed in films of PFO-wrapped s-SWCNTs[24] and significantly bigger than ~0.34 nm distance in bundles of bare nanotubes that lack polymer wrapping. The same measurements for sample fabricated by CPD give wall-to-wall distance of 0.5 ± 0.2 nm.

These distances would appear to be in agreement with what is expected from the intrafiber exciton transfer rates derived above. However, there are many uncertainties in these wall-to-wall distances that are hard to quantify. For example, our analysis assumes that the nanotubes are in the same plane perpendicular to the electron beam of the TEM, but the fibers could be oriented at an angle such that the nanotubes are not at the same height. Any angle other than perpendicular will produce a smaller wall-to-wall distance. Another issue is the contrast. The distances were measured at positions with high contrast, with the assumption that the positions correspond to the walls of the nanotubes, but it is not clear how the polymer modulates the contrast. Finally, the sample may drift in the focus during the measurement, which is difficult to control. Clearly, more experiments are needed to

elucidate the internal structure of the fibers. Nonetheless, these kinetics experiments suggest that the tubes in fibers produced by CPD are indeed closer.

Other Factors That Can Influence the Transfer Rates. The pump–probe experiments reported here are ensemble measurements and so the extracted rate constants are average properties. As such, one might expect there to be significant variations from these quantities. For example, the polymer wrapping may not be equally dispersed along the nanotubes, thereby allowing the nanotube separation to vary along the lengths of the fibers. Indeed, the TEM images of the fibers are not uniform (Figure 9a,b); there are regions in which the tubes are not individually discernible, possibly indicating a larger amount of polymer wrapping. If so, the intrafiber rate constant fit from these experiments may be dominated by high transfer probabilities that occur at relatively infrequent but narrow separations.

Along these lines, we point out that we measured the wall-to-wall distances in fibers composed of 2 or 3 tubes, whereas most fibers contain tens of tubes. Fibers with only 2 or 3 tubes appear in only about 10% of the TEM images collected. Thus, they are not common and may not be representative of the wall-to-wall distances in the majority of fibers. Nonetheless, the trend to smaller distances in CPD does agree with the predictions from the rate constants.

Another consideration not included in our model is the line widths. The E_{11} transitions have ≈30% narrower line widths in the CPD films than in the doctor-bladed films. Narrower line widths can result in better spectral overlap between resonant E_{11} transition of (7,5) and phonon sideband of (8,7), which in turn would enhance energy transfer between these tubes, depending on the mechanism. Further experiments under varying film conditions should help ascertain the importance of each of the factors above for exciton transfer in films like these.

CONCLUSION

We use ultrafast transient absorption spectroscopy to study kinetics of exciton migration in s-SWCNT thin films. In these films, excitons are transferred from smaller to larger diameter tubes as well as between tubes of the same band gap on femtosecond-to-picosecond time scales. In the dense doctor-bladed films, both intra- and interfiber hopping occurs, whereas in the very porous CPD films, interfiber transfer is greatly suppressed. Of the models considered here, only model 4 explains the data in which transfer between bundles occurs at intersections where the tubes are close to touching. Diffusion to these intersections is a key component of this model. Exciton diffusion in carbon nanotubes is exceedingly fast, and so the excitons can travel large distances to find an intersection during their lifetime. It was surprising to us that intersections can play such an important role since we had expected hopping to be more efficient between nanotubes within fibers in which the tubes are parallel over large distances. This result, which stems from the anisotropy measurements and is independent of the modeling, might be a consequence of gaps in the polymer wrapping that allow tubes to come into close proximity at fiber–fiber intersections. Nonetheless, the exciton transfer dynamics in semiconducting carbon nanotube films of these types can be effectively understood and modeled using the approach outlined here, over a very wide range of tube distances and densities. Accordingly, these results provide a better understanding of the physics of exciton migration that is essential for the rational design of photovoltaic and electroluminescent devices using these exciting new materials.

METHODS

Details on nanotube preparation, doctor-blade casting of s-SWCNTs films and transient absorption spectroscopy are reported elsewhere.[29] CPD films are prepared by the following procedure. s-SWCNTs solutions were mixed with 2 wt % poly(methyl methacrylate) (PMMA)/chlorobenze solution at a ratio of 1:1 and deposited onto indium tin oxide (ITO)-coated glass substrates using a drop-casting method. The PMMA was then removed by repeated rinsing in acetone and isopropyl alcohol (IPA). The resulting nanotube films were quickly transferred to the chamber of a critical point dryer (Automegasamdri 915B) filled with IPA. The films were maintained in a wet state during transfer. The IPA bath solution was then purged for 8 min in exchange for liquid CO_2 under 800 psi. The chamber pressure was raised to 1300 psi, and the temperature was raised to above 38 °C to reach the critical state. The nanotube films were thus dried without introducing any surface-tension-induced bundling, resulting in a highly porous network structure.

For TEM measurements, we use a mixture enriched in (7,5) tubes. Doctor-bladed samples for TEM are prepared by the following procedure. The nanotubes are deposited onto ITO using doctor-blade casting. The sample is then immersed into hydrochloric acid (HCl, 12 M, Fisher Scientific) for 1 min. After the ITO substrate is dissolved, the nanotube film is transferred three times into deionized water and soaked for 1 min each time. Finally, the film is transferred onto a TEM grid and dried under air. CPD samples for TEM are prepared by gently pressing a TEM grid against a CPD-deposited film. After separation, the film is attached to the grid. Carbon nanotube films were imaged using an FEI Tecnai T12 transmission electron microscope with an accelerating voltage of 120 kV.

Conflict of Interest: The authors declare no competing financial interest.

Acknowledgment. Funding was provided by AFOSR FA9550-12-1-0063. Additional funding was provided for M.-Y. W. by UW-CEMRI DMR-1121288, R.D.M. by the DoD, Air Force Office of Scientific Research, National Defense Science and Engineering Graduate (NDSEG) Fellowship, 32 CFR 168a, T.J.M. by the NSF Graduate Research Fellowship Program (DGE-1256259), Y.Y. by NSF-CBET-1033346, and R.M.J. by the DOE Office of Science Early Career Research Program (Grant No. DE- SC0006414) through

the Office of Basic Energy Sciences, for TEM measurements, and from the Department of Defense (DOD) through the National Defense Science & Engineering Graduate Fellowship (NDSEG) Program.

Supporting Information Available: Figures showing absorbance and photoluminescence spectra for sample B; TEM images of CPD-prepared film and small fibers produced by doctor-blading and CPD; anisotropy kinetics for samples A and C; kinetics traces simulated using models 1−3 with ratio of inter- to intrafiber transfer rate constants of 1/3 and 1/10; anisotropy kinetics simulated for sample B using model 1 with angle-independent interfiber transfer. Derivation of master equations and derivation of time dependence for transfer rate constants in model 4. This material is available free of charge *via* the Internet at http://pubs.acs.org.

REFERENCES AND NOTES

1. Arnold, M. S.; Green, A. A.; Hulvat, J. F.; Stupp, S. I.; Hersam, M. C. Sorting Carbon Nanotubes by Electronic Structure Using Density Differentiation. *Nat. Nanotechnol.* **2006**, *1*, 60–65.
2. Khripin, C. Y.; Fagan, J. A.; Zheng, M. Spontaneous Partition of Carbon Nanotubes in Polymer-Modified Aqueous Phases. *J. Am. Chem. Soc.* **2013**, *135*, 6822–6825.
3. Lebedkin, S.; Hennrich, F.; Kiowski, O.; Kappes, M. M. Photophysics of Carbon Nanotubes in Organic Polymer−Toluene Dispersions: Emission and Excitation Satellites and Relaxation Pathways. *Phys. Rev. B* **2008**, 77.
4. Liu, H.; Nishide, D.; Tanaka, T.; Kataura, H. Large-Scale Single-Chirality Separation of Single-Wall Carbon Nanotubes by Simple Gel Chromatography. *Nat. Commun.* **2011**, 2.
5. Nish, A.; Hwang, J. Y.; Doig, J.; Nicholas, R. J. Highly Selective Dispersion of Singlewalled Carbon Nanotubes Using Aromatic Polymers. *Nat. Nanotechnol.* **2007**, *2*, 640–646.
6. Bernardi, M.; Lohrman, J.; Kumar, P. V.; Kirkeminde, A.; Ferralis, N.; Grossman, J. C.; Ren, S. Nanocarbon-Based Photovoltaics. *ACS Nano* **2012**, *6*, 8896–8903.
7. Bindl, D. J.; Safron, N. S.; Arnold, M. S. Dissociating Excitons Photogenerated in Semiconducting Carbon Nanotubes at Polymeric Photovoltaic Heterojunction Interfaces. *ACS Nano* **2010**, *4*, 5657–5664.
8. Bindl, D. J.; Shea, M. J.; Arnold, M. S. Enhancing Extraction of Photogenerated Excitons from Semiconducting Carbon Nanotube Films as Photocurrent. *Chem. Phys.* **2013**, *413*, 29–34.
9. Jain, R. M.; Howden, R.; Tvrdy, K.; Shimizu, S.; Hilmer, A. J.; McNicholas, T. P.; Gleason, K. K.; Strano, M. S. Polymer-Free Near-Infrared Photovoltaics with Single Chirality (6,5) Semiconducting Carbon Nanotube Active Layers. *Adv. Mater.* **2012**, *24*, 4436–4439.
10. Kazaoui, S.; Minami, N.; Nalini, B.; Kim, Y.; Hara, K. Near-Infrared Photoconductive and Photovoltaic Devices Using Single-Wall Carbon Nanotubes in Conductive Polymer Films. *J. Appl. Phys.* **2005**, *98*, 084314-6.
11. Ramuz, M. P.; Vosgueritchian, M.; Wei, P.; Wang, C.; Gao, Y.; Wu, Y.; Chen, Y.; Bao, Z. Evaluation of Solution-Processable Carbon-Based Electrodes for All-Carbon Solar Cells. *ACS Nano* **2012**, *6*, 10384–10395.
12. Svrcek, V.; Cook, S.; Kazaoui, S.; Kondo, M. Silicon Nanocrystals and Semiconducting Single-Walled Carbon Nanotubes Applied to Photovoltaic Cells. *J. Phys. Chem. Lett.* **2011**, *2*, 1646–1650.
13. Tung, V. C.; Huang, J.-H.; Tevis, I.; Kim, F.; Kim, J.; Chu, C.-W.; Stupp, S. I.; Huang, J. Surfactant-Free Water-Processable Photoconductive All-Carbon Composite. *J. Am. Chem. Soc.* **2011**, *133*, 4940–4947.
14. Misewich, J. A.; Martel, R.; Avouris, P.; Tsang, J. C.; Heinze, S.; Tersoff, J. Electrically Induced Optical Emission from a Carbon Nanotube FET. *Science* **2003**, *300*, 783–786.
15. Crochet, J. J.; Sau, J. D.; Duque, J. G.; Doorn, S. K.; Cohen, M. L. Electrodynamic and Excitonic Intertube Interactions in Semiconducting Carbon Nanotube Aggregates. *ACS Nano* **2011**, *5*, 2611–2618.
16. Wong, C. Y.; Curutchet, C.; Tretiak, S.; Scholes, G. D. Ideal Dipole Approximation Fails to Predict Electronic Coupling and Energy Transfer between Semiconducting Single-Wall Carbon Nanotubes. *J. Chem. Phys.* **2009**, *130*, 081104-4.
17. Wu, M.-Y.; Jacobberger, R. M.; Arnold, M. S. Design Length Scales for Carbon Nanotube Photoabsorber Based Photovoltaic Materials and Devices. *J. Appl. Phys.* **2013**, *113*, 204504-15.
18. Lefebvre, J.; Finnie, P. Photoluminescence and Forster Resonance Energy Transfer in Elemental Bundles of Single-Walled Carbon Nanotubes. *J. Phys. Chem. C* **2009**, *113*, 7536–7540.
19. Qian, H.; Georgi, C.; Anderson, N.; Green, A. A.; Hersam, M. C.; Novotny, L.; Hartschuh, A. Exciton Energy Transfer in Pairs of Single-Walled Carbon Nanotubes. *Nano Lett.* **2008**, *8*, 1363–1367.
20. Tan, P. H.; Rozhin, A. G.; Hasan, T.; Hu, P.; Scardaci, V.; Milne, W. I.; Ferrari, A. C. Photoluminescence Spectroscopy of Carbon Nanotube Bundles: Evidence for Exciton Energy Transfer. *Phys. Rev. Lett.* **2007**, *99*, 137402.
21. Kato, T.; Hatakeyama, R. Exciton Energy Transfer-Assisted Photoluminescence Brightening from Freestanding Single-Walled Carbon Nanotube Bundles. *J. Am. Chem. Soc.* **2008**, *130*, 8101–8107.
22. Chen, F.; Ye, J.; Teo, M. Y.; Zhao, Y.; Tan, L. P.; Chen, Y.; Chan-Park, M. B.; Li, L.-J. Species-Dependent Energy Transfer of Surfactant-Dispersed Semiconducting Single-Walled Carbon Nanotubes. *J. Phys. Chem. C* **2009**, *113*, 20061–20065.
23. Han, J.-H.; Paulus, G. L. C.; Maruyama, R.; Heller, D. A.; Kim, W.-J.; Barone, P. W.; Lee, C. Y.; Choi, J. H.; Ham, M.-H.; Song, C.; *et al.* Exciton Antennas and Concentrators from Core-Shell and Corrugated Carbon Nanotube Filaments of Homogeneous Composition. *Nat. Mater.* **2010**, *9*, 833–839.
24. Koyama, T.; Miyata, Y.; Asada, Y.; Shinohara, H.; Kataura, H.; Nakamura, A. Bright Luminescence and Exciton Energy Transfer in Polymer-Wrapped Single-Walled Carbon Nanotube Bundles. *J. Phys. Chem. Lett.* **2010**, *1*, 3243–3248.
25. Koyama, T.; Miyata, Y.; Asaka, K.; Shinohara, H.; Saito, Y.; Nakamura, A. Ultrafast Energy Transfer of One-Dimensional Excitons between Carbon Nanotubes: A Femtosecond Time-Resolved Luminescence Study. *Phys. Chem. Chem. Phys.* **2012**, *14*, 1070–1084.
26. Luer, L.; Crochet, J.; Hertel, T.; Cerullo, G.; Lanzani, G. Ultrafast Excitation Energy Transfer in Small Semiconducting Carbon Nanotube Aggregates. *ACS Nano* **2010**, *4*, 4265–4273.
27. Maeda, A.; Matsumoto, S.; Kishida, H.; Takenobu, T.; Iwasa, Y.; Shimoda, H.; Zhou, O.; Shiraishi, M.; Okamoto, H. Gigantic Optical Stark Effect and Ultrafast Relaxation of Excitons in Single-Walled Carbon Nanotubes. *J. Phys. Soc. Jpn.* **2006**, *75*, 043709.
28. Bindl, D. J.; Wu, M.-Y.; Prehn, F. C.; Arnold, M. S. Efficiently Harvesting Excitons from Electronic Type-Controlled Semiconducting Carbon Nanotube Films. *Nano Lett.* **2011**, *11*, 455–460.
29. Mehlenbacher, R. D.; Wu, M.-Y.; Grechko, M.; Laaser, J. E.; Arnold, M. S.; Zanni, M. T. Photoexcitation Dynamics of Coupled Semiconducting Carbon Nanotube Thin Films. *Nano Lett.* **2013**, *13*, 1495–1501.
30. Bryning, M. B.; Milkie, D. E.; Islam, M. F.; Hough, L. A.; Kikkawa, J. M.; Yodh, A. G. Carbon Nanotube Aerogels. *Adv. Mater.* **2007**, *19*, 661–664.
31. Soavi, G.; Scotognella, F.; Brida, D.; Hefner, T.; Spath, F.; Antognazza, M. R.; Hertel, T.; Lanzani, G.; Cerullo, G. Ultrafast Charge Photogeneration in Semiconducting Carbon Nanotubes. *J. Phys. Chem. C* **2013**, *117*, 10849–10855.
32. Harrah, D. M.; Schneck, J. R.; Green, A. A.; Hersam, M. C.; Ziegler, L. D.; Swan, A. K. Intensity-Dependent Exciton Dynamics of (6,5) Single-Walled Carbon Nanotubes: Momentum Selection Rules, Diffusion, and Nonlinear Interactions. *ACS Nano* **2011**, *5*, 9898–9906.
33. Scholes, G. D. Long-Range Resonance Energy Transfer in Molecular Systems. *Annu. Rev. Phys. Chem.* **2003**, *54*, 57–87.
34. Ando, T. Environment Effects on Excitons in Semiconducting Carbon Nanotubes. *J. Phys. Soc. Jpn.* **2010**, *79*, 024706.

35. Hagen, A.; Steiner, M.; Raschke, M. B.; Lienau, C.; Hertel, T.; Qian, H.; Meixner, A. J.; Hartschuh, A. Exponential Decay Lifetimes of Excitons in Individual Single-Walled Carbon Nanotubes. *Phys. Rev. Lett.* **2005**, *95*, 197401.
36. Ma, Y.-Z.; Stenger, J.; Zimmermann, J.; Bachilo, S. M.; Smalley, R. E.; Weisman, R. B.; Fleming, G. R. Ultrafast Carrier Dynamics in Single-Walled Carbon Nanotubes Probed by Femtosecond Spectroscopy. *J. Chem. Phys.* **2004**, *120*, 3368–3373.
37. Wang, F.; Dukovic, G.; Brus, L. E.; Heinz, T. F. Time-Resolved Fluorescence of Carbon Nanotubes and Its Implication for Radiative Lifetimes. *Phys. Rev. Lett.* **2004**, *92*, 177401.
38. Zhao, H.; Mazumdar, S. Electron−Electron Interaction Effects on the Optical Excitations of Semiconducting Single-Walled Carbon Nanotubes. *Phys. Rev. Lett.* **2004**, *93*, 157402.
39. Crochet, J. J.; Duque, J. G.; Werner, J. H.; Lounis, B.; Cognet, L.; Doorn, S. K. Disorder Limited Exciton Transport in Colloidal Single-Wall Carbon Nanotubes. *Nano Lett.* **2012**, *12*, 5091–5096.
40. Hertel, T.; Himmelein, S.; Ackermann, T.; Stich, D.; Crochet, J. Diffusion Limited Photoluminescence Quantum Yields in 1-D Semiconductors: Single-Wall Carbon Nanotubes. *ACS Nano* **2010**, *4*, 7161–7168.
41. Lefebvre, J.; Austing, D. G.; Bond, J.; Finnie, P. Photoluminescence Imaging of Suspended Single-Walled Carbon Nanotubes. *Nano Lett.* **2006**, *6*, 1603–1608.
42. Cognet, L.; Tsyboulski, D. A.; Rocha, J.-D. R.; Doyle, C. D.; Tour, J. M.; Weisman, R. B. Stepwise Quenching of Exciton Fluorescence in Carbon Nanotubes by Single-Molecule Reactions. *Science* **2007**, *316*, 1465–1468.
43. Georgi, C.; Böhmler, M.; Qian, H.; Novotny, L.; Hartschuh, A. Probing Exciton Propagation and Quenching in Carbon Nanotubes with Near-Field Optical Microscopy. *Phys. Status Solidi B* **2009**, *246*, 2683–2688.
44. Siitonen, A. J.; Tsyboulski, D. A.; Bachilo, S. M.; Weisman, R. B. Surfactant-Dependent Exciton Mobility in Single-Walled Carbon Nanotubes Studied by Single-Molecule Reactions. *Nano Lett.* **2010**, *10*, 1595–1599.
45. Moritsubo, S.; Murai, T.; Shimada, T.; Murakami, Y.; Chiashi, S.; Maruyama, S.; Kato, Y. K. Exciton Diffusion in Air-Suspended Single-Walled Carbon Nanotubes. *Phys. Rev. Lett.* **2010**, *104*, 247402.
46. Crochet, J. J.; Duque, J. G.; Werner, J. H.; Doorn, S. K. Photoluminescence Imaging of Electronic-Impurity-Induced Exciton Quenching in Single-Walled Carbon Nanotubes. *Nat. Nanotechnol.* **2012**, *7*, 126–132.
47. Yoshikawa, K.; Matsuda, K.; Kanemitsu, Y. Exciton Transport in Suspended Single Carbon Nanotubes Studied by Photoluminescence Imaging Spectroscopy. *J. Phys. Chem. C* **2010**, *114*, 4353–4356.
48. Anderson, M. D.; Xiao, Y.-f.; Fraser, J. M. First-Passage Theory of Exciton Population Loss in Single-Walled Carbon Nanotubes Reveals Micron-Scale Intrinsic Diffusion Lengths. *Phys. Rev. B* **2013**, *88*, 045420.
49. Collins, F. C.; Kimball, G. E. Diffusion-Controlled Reaction Rates. *J. Colloid Sci.* **1949**, *4*, 425–437.
50. Rice, S. A. *Diffusion-Limited Reactions*; Elsevier: Amsterdam, 1985; Vol. 25, p 404.
51. Luer, L.; Hoseinkhani, S.; Polli, D.; Crochet, J.; Hertel, T.; Lanzani, G. Size and Mobility of Excitons in (6,5) Carbon Nanotubes. *Nat. Phys.* **2009**, *5*, 54–58.